Simulation of Vortex–Dominated Flows Using the FLASH Code

Vikram Dwarkadas,[1] Tomek Plewa,[1] Greg Weirs,[1] Chris Tomkins,[2] and Mark Marr-Lyon[2]

[1] ASCI FLASH Center, University of Chicago `vikram@flash.uchicago.edu`, `tomek@flash.uchicago.edu`, `weirs@flash.uchicago.edu`

[2] Los Alamos National Laboratory `ctomkins@lanl.gov`, `mmarr@lanl.gov`

1 Abstract

We compare the results of two–dimensional simulations to experimental data obtained at Los Alamos National Laboratory in order to validate the FLASH code. FLASH is a multi–physics, block–structured adaptive mesh refinement code for studying compressible, reactive flows in various astrophysical environments. The experiment involves the lateral interaction between a planar Ma=1.2 shock wave with a cylinder of gaseous sulfur hexafluoride (SF_6) in air. The development of primary and secondary flow instabilities after the passage of the shock, as observed in the experiments and numerical simulations, are reviewed and compared. The sensitivity of numerical results to several simulation parameters are examined. Computed and experimentally measured velocity fields are compared. Motivation for experimental data in planes parallel to the cylinder axis is provided by a speculative three–dimensional simulation.

2 Introduction

The impulsive acceleration of a material interface can lead to complex fluid motions due to the Richtmyer–Meshkov (RM) instability. Here, the misalignment of pressure and density gradients deposits vorticity along the interface, which drives the flow and distorts the interface. At later times the flow may be receptive to secondary instabilities, most prominently the Kelvin–Helmholtz instability, which further increase the flow complexity and may trigger transition to turbulence.

Experimental investigations of impulsively accelerated interfaces have focused mainly on interfaces with single–mode perturbations, and on the case we consider here, shock–accelerated cylindrical gas columns [1, 2, 3]. The experiments are relatively inexpensive and turnaround times are short. The

challenges are diagnostics and repeatability: after the shock passes, the flow-field evolution is driven by flow instabilities and vortex dynamics, which are sensitive to the initial conditions and noise in the system. Specifically, for the present case of a single shock–accelerated gas cylinder, the flow is dominated by a counter–rotating vortex pair.

Verification and validation are critical in the development of any simulation code, without which one can have little confidence that the code's results are meaningful. The sensitivity and the complex evolution of the vortex pair are desirable properties for our primary purpose, which is to use the experiments to validate our simulation code. A well–designed, well–characterized, and accurately diagnosed experiment is essential for validation.

FLASH is a multi–species, multi–dimensional, parallel, adaptive–mesh–refinement, fluid dynamics code for applications in astrophysics [4]. Calder et al. discuss initial validation tests of the FLASH code [5]. Herein we continue our validation effort by comparing FLASH simulations to an experiment performed at the Los Alamos National Laboratories [2, 3].

3 Two–Dimensional Simulations

3.1 Experimental Facility and Initial Conditions

The experimental apparatus is a shock–tube with a 7.5 cm square cross–section. Gaseous SF_6 flows from an 8 mm diameter nozzle in the top wall of the shock–tube, forming a cylinder of dense gas in the otherwise air–filled test section. A Ma=1.2 shockwave travels through the shock–tube and passes through the cylinder. Our interest is in the resulting evolution of the SF_6. The experiment is nominally two–dimensional, and the experimental data are taken in a plane normal to the cylinder axis.

The initial SF_6 distribution (before the shock impact) is visualized by Rayleigh–Scattering from the SF_6 molecules [2]. The image plane is 2 cm below the top wall of the test section. As the SF_6 flows downward, air diffuses into the SF_6 column, reducing the peak concentration of the heavy gas. One limitation of the visualization technique is that the pixel intensity in the images gives only the mole fraction of SF_6 relative to the peak mole fraction. The scaling between pixel intensity and mole fraction is linear, with the proportionality constant specified by the maximum initial mole fraction of SF_6, denoted X_{SF6}.

After shock passage, two–dimensional velocity vectors in a plane are obtained using particle image velocimetry (PIV) [6]. The technique yields high resolution (spacing between vectors is about 187 microns) and high accuracy (measurement error is 1.5% of the structure convection velocity). Raw images are interrogated using a two-frame cross-correlation technique [7], which produces approximately 3600 vectors per realization. For PIV both the air and the SF_6 must be seeded with water/glycol droplets, nominally 0.5 μm in

diameter, the displacement of which is used to obtain velocity data—hence, simultaneous velocity and composition images cannot be obtained.

The 608×468 pixel image of the initial SF_6 distribution is shown in Fig. 1. The pixel size is 38 microns when projected into the measurement plane. The pixel intensity is plotted, with 20 contours equally spaced between values of 5 and 165. The deformation of the contours indicates that the distribution of SF_6, as revealed by the diagnostics, is only approximately radially symmetric. Also, the signal is completely dominated by noise at the level of about 5–10% (the two lowest density contours in Fig. 1). Since the asymmetries are likely to vary from one experimental shot to another and the flowfield evolution is highly sensitive to noise, smooth initial conditions for our simulations are obtained by fitting a radially–symmetric function to the experimental data.
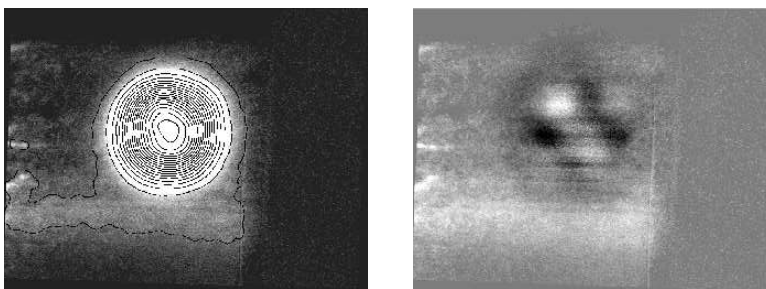

Fig. 1. (a) The initial conditions for the single–cylinder experiment with an 8mm nozzle. (b) Residuals between the experimental image and the composite Gaussian fit. The scale varies from -10 (black) to +10 (white) in intensity units. The maximum signal in the image has an intensity of about 165. Note a semi–regular non–radial m=4,l=4 component with maximum signal reaching about 10% of local intensity.

To obtain the smooth initial conditions we used the MINGA minimization package [8]. The fit extended out to a radius of 150 pixels from the center. After examining many trial functions, we selected the form:

$$C(r) = u_1 e^{(-r^2/u_2^2)} + u_3 e^{(-r^2/u_4^2)} + u_5 e^{(-(r-u_6)^2/u_7^2)} + u_8 e^{(-(r-u_9)^2/u_{10}^2)}$$

where $u_1 = 144.0725$, $u_2 = 69.45422$, $u_3 = 9.221577$, $u_4 = 20.10299$, $u_5 = 32.47960$, $u_6 = 42.59238$, $u_7 = 32.10067$, $u_8 = -1.559247$, $u_9 = 98.27106$, and $u_{10} = 15.51837$. (The length units are pixels, and the maximum intensity will be rescaled to X_{SF6}.) Residuals are shown in Fig. 1. The experimental data appears to contain a significant non–radial signal which can be characterized by an m=4, l=4 perturbation with an amplitude of about 10%. Our fit does not account for this additional component.

3.2 Overview of the Simulations

As the shock travels, it accelerates the medium through which it propagates. As the shock traverses the cylinder, vorticity is deposited baroclinically along the interface, i.e., due to the misalignment of the pressure gradient (normal to the shock) and the density gradient (normal to the interface.) The vorticity deposition is not uniform: it is maximum when the gradients are perpendicular, and since the shock is slowed in the SF_6, the maximum is shifted to the downstream portion of the cylinder edge. Once the shock has passed through the SF_6, vorticity generation due to the primary instability is complete. The existing vorticity drives the flow: a counter–rotating vortex pair forms, then rolls up. The vortex Reynolds number of the flow, as measured experimentally, is Re= $\Gamma/\nu \approx 5 \times 10^4$. The development and evolution of the vortex pair and subsequent instabilities at the interface proceed in a weakly compressible regime. More precise descriptions can be found in the references [1, 9, 3].

Figure 2 shows a sequence of images from our baseline simulation. The minimum grid resolution is 78 microns, the initial peak mole fraction of SF_6 is 0.6, and the Courant (CFL) number is 0.8. (The CFL number is a nondimensional measure of the timestep size.) For all simulations, the streamwise and spanwise extent of the domain were 64 cm and 8 cm, respectively. Overall the flow features in the simulation results are similar to those in the experimentally obtained images. Next we will describe the effects of several simulation parameters on the computed results. The amount and location of small–scale structure, relative to the experimental data, is used as a qualitative metric.

| 0 | 50 | 190 | 330 | 470 | 610 | 750 |

Fig. 2. Evolution of the SF_6, with time elapsed after shock impact listed in μs. The mass fraction of SF_6 is shown, with X_{SF6}=0.6 and CFL=0.8.

3.3 Effects of Simulation Parameters

Effect of Maximum Initial Mole Fraction

Because the experimental images provide only information about the relative mole fractions, the maximum mole fraction of SF_6 at the start of the simulation is a free parameter in our initial conditions. We have focused on two values, X_{SF6}=0.8, motivated by experimental estimates, and X_{SF6}=0.6,

better supported by comparison of simulation and experimental results. Simulation results are presented in Fig. 3. For X_{SF6}=0.8, the numerical solution shows excessive small–scale structure compared to the experimental data.

$$X_{SF_6}=0.6 \qquad X_{SF_6}=0.8$$

Fig. 3. SF_6 mass fraction at $750\mu s$ after shock impact. Initial maximum SF_6 mole fraction X_{SF6}=0.6 on the left, and on the right X_{SF6}=0.8.

Effect of Grid Resolution

Using FLASH's adaptive mesh refinement capability, we have run simulations at three grid resolutions. Results at 750 μs are presented in Fig. 4, with minimum grid spacings of 156 microns, 78 microns and 39 microns. We observe that the amount of small–scale structure increases on finer grids. This can be understood since the numerical dissipation in FLASH's shock–capturing scheme (PPM) is resolution dependent, and no physical viscosity model was used for these simulations. (Estimates of the length scale of molecular diffusion at the flow conditions of the experiment are below 10 microns.) At a grid resolution of 39 microns, the primary vortex cores are not easily identified among the diffuse, turbulent structures. At the lower resolutions, the two primary vortex cores are unambiguous.

$$dx=156 \qquad dx=78 \qquad dx=39$$

Fig. 4. SF_6 mass fraction at 750 μs with increasing grid resolution, labeled in microns. At the highest level of resolution, the vortex cores appear diffuse.

Flow–Mesh Interaction

It is known that unavoidable interpolation errors near discontinuous jumps in grid resolution can act as sources of spurious small–scale structure [10]. To test this possibility we have run simulations in which a predetermined area around the vortices is uniformly refined to the highest resolution. Compared to fully adaptive refinement (the default) this approach significantly reduces the amount of perturbations introduced by the grid adaption process.

In Fig. 5 we compare the results from a fully adaptive grid and grids with maximally refined rectangles of 3×3 cm, 4×4 cm, and 4×8 cm. The vortex structure is always less than 2 cm across. The results are shown at 750 μs after shock impact. For all grids, the minimum grid spacing is 78 microns and the CFL number is 0.8. For the different grids the large scale morphology, such as size of the cylinder cross–section and the basic vortex structure, remains the same. However, the shape of the cross–section visibly differs depending on the grid, as does the amount and location of small–scale structures. In particular, differences are noticeable in the small–scale instabilities present on the vortex rolls. Since all other simulation aspects are the same, the differences must originate with perturbations at jumps in refinement.
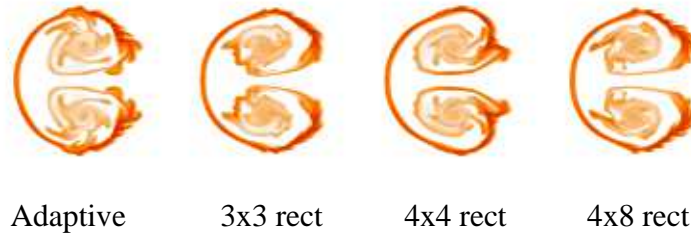

Adaptive   3x3 rect   4x4 rect   4x8 rect

Fig. 5. Solutions on different grids, 750 μs after shock impact at CFL=0.8. Left to right: fully adaptive grid; 3×3 cm refined rectangle; 4×4 cm refined rectangle; 4×8 cm refined rectangle. In the rightmost image, the refined rectangle covers the entire spanwise extent of the test section.

Effect of Courant Number

The timestep in an explicit hydrodynamic code is limited by the CFL number. In general we use a value of CFL=0.8, but we have also performed simulations with the time step size limited by CFL=0.2. Reducing the timestep generally reduces the temporal truncation error; however, it might have an adverse effect on the spatial error. Additionally the mesh can adapt more often per unit of simulation time, and if errors are committed every time the mesh adapts, this could lead to a less accurate solution.

We repeated the simulations described above, but at CFL=0.2. The results are shown in Fig. 6. The simulations at CFL=0.2 are much less sensitive to grid adaption: there is much less variation between solutions on adaptive and locally uniform grids at CFL=0.2 than at CFL=0.8. One explanation for these results is that the errors at the fine–coarse boundaries are larger and lead to stronger perturbations at higher CFL numbers. An alternative explanation is that at higher Courant numbers, PPM does not adequately compute solutions at these conditions. Our simulations indicate that for FLASH, a lower CFL number is preferred in this regime.

Our fully adaptive grid simulations provides a speed–up factor of about 10, compared to the grids with the 4×8 cm maximally refined rectangle. Such large savings demonstrate the advantages of adaptive mesh refinement. At the same time, caution is warranted: our results also demonstrate that AMR generates perturbations which, depending on other simulation parameters and the flow regime, can give rise to spurious small–scale structures.
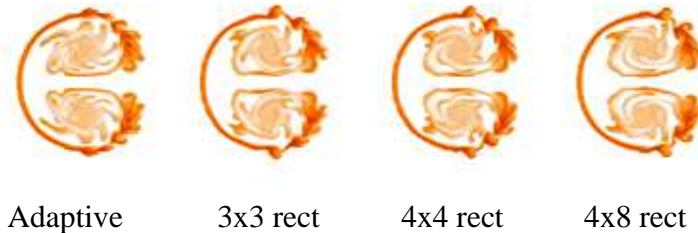

Adaptive   3x3 rect   4x4 rect   4x8 rect

Fig. 6. Solutions on different grids for CFL=0.2; for other details see Fig. 5.

3.4 Metrics for Comparison to Experimental Data

Evolution of Cylinder Size

In Fig. 7 we present integral scale measures – the streamwise and spanwise extent of the SF_6 – over time. The contour of SF_6 mass fraction equal to 0.1 was used to define the edge of the SF_6. We plot results for our baseline simulation and simulations where a single parameter is varied relative to the baseline. For a given maximum initial SF_6 mole fraction, the cylinder height and width are essentially insensitive to the parameters varied. These integral measures provide a basis for comparison of our simulation results to those of others (e.g. [3, 11]), as well as to the experimental data.

Velocity Comparisons

We compare the magnitude of the velocity fluctuations from the experimental data to that from the simulation results. The velocity fluctuation is defined as
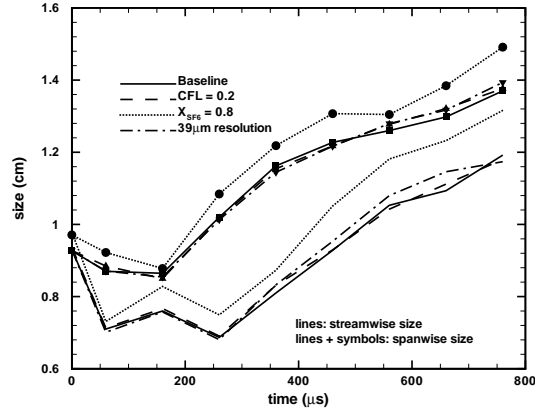
Fig. 7. Integral scale measures plotted at nine simulation times. For the baseline case, X_{SF6}=0.6, CFL=0.8, and 78 micron resolution. For other cases a single parameter varies from the baseline case.

the velocity in the frame of reference of the vortices. To find the velocity fluctuation we subtract the convective velocity, which we define as the streamwise velocity component in the lab frame at the point of the maximum vorticity.

The experimental data are the velocity components and the corresponding vorticity on 60×60 points uniformly covering a 12×12 mm region around one of the primary vortices. We find the convective velocity to be 101.25 m/s. The magnitude of the velocity fluctuations are plotted as flooded contours in the left plot of Fig. 8, together with streamlines of the velocity fluctuations. The plot is oriented such that the shock has passed through the image from top to bottom, and the centerline (between the primary vortices) is near the right edge of the plot.

The right plot of Fig. 8 shows the same quantities but from the simulation data (78 micron resolution, X_{SF6}=0.6, CFL=0.2), for which the convective velocity is 92.90 m/s. The velocity fluctuation field in the simulations compares reasonably well to the experimental data. The maximum and minimum fluctuations occur in approximately the same places. The velocities in the simulation are up to 10% higher than in the experiment. The simulation data shows more structure, and there is some (visual, at least) correlation between the structure in the velocity fluctuations and the SF_6 distribution.

4 Three–Dimensional Simulation

While the experiment is nominally two–dimensional, several factors might contribute to non–negligible three–dimensional effects. Probably the most significant experimental deviations from two–dimensionality are due to the diffusion of the SF_6 as it flows from the top of the test section to the bottom. As a
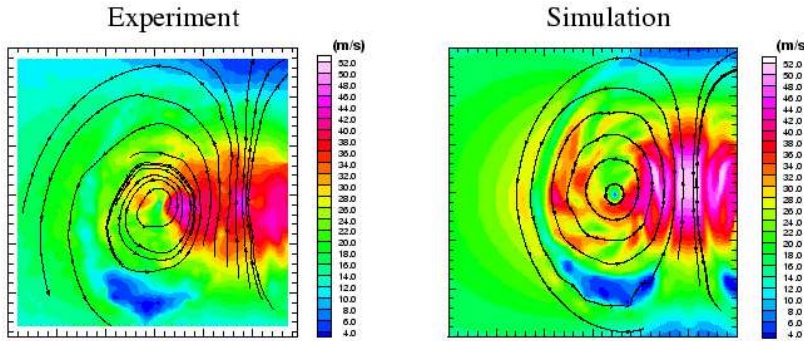
Experiment   Simulation

Fig. 8. Velocity fluctuation magnitude and streamlines around one primary vortex 750 μs after shock impact. The shock has passed through the image from the top to bottom. Left: experimental data. Right: simulation data.

result, the mixture composition and density vary with height. (This is why we assume the maximum initial mole fraction of SF_6 is less than 1.0 in the two–dimensional simulations.) Even if the cylinder were invariant with height, the flowfield after the shock passes the cylinder is dominated by vorticity dynamics, and small scale structures arising from flow instabilities eventually develop at the vortex edges. The effects of such inherently three–dimensional phenomena cannot be captured in two–dimensional simulations.

We executed a speculative three–dimensional simulation which, though it cannot definitively establish that three–dimensional effects are essential for the shock–cylinder interaction, compels further experimental and computational investigation. Our z-direction extension of the initial conditions is purely ad hoc, because we have no corresponding experimental data. Of course, this simulation cannot be used as a validation test for the FLASH code, but we hope it will open a new line of investigation and discussion.

For this simulation the z-direction is parallel to the cylinder axis, with z=0.0 cm at the bottom wall and z=8.0cm at the top wall. To initialize the flowfield, we begin with the "raw" image in Fig. 1. Only after this simulation was completed did we learn that the raw images have spurious high frequency noise, and smooth approximations to the raw data are believed to better represent the true SF_6 field [2]. The streamwise (x) and spanwise (y) dimensions of the image are rescaled linearly with z, so the SF_6 covers a smaller area at the top wall and a larger area at the bottom. Consequently the maximum mole fraction of SF_6 in each plane varies as z^2, and is 0.64 at the top wall and 0.47 at the z=6.0 cm plane, at which the "raw" image was obtained. Otherwise the initialization is the same as for the two–dimensional simulations. The simulation was run at CFL=0.8 using fully adaptive mesh refinement, and the minimum grid spacing was 156 microns in all three spatial dimensions.

Near the top wall in our simulation, the vortices have rolled up more than at the bottom, and more small scale structure has developed. This observation appears to hold throughout the course of the simulation, and can be understood as follows. The rescaling of the initial SF_6 distribution results in larger composition gradients, and correspondingly larger density gradients, near the top and smaller gradients near the bottom. The primary source of vorticity generation in this problem is through baroclinic torque, so more vorticity is deposited near the upper wall, where the density gradients are largest.

The circulation provides a quantitative measure of the vortex development. The z-component of circulation was calculated for the lower-y half of each xy-plane of the simulation, bounded by the centerline, y=0.0 cm, and the inflow and outflow boundaries. Figure 9 shows the circulation at z=0.0, 2.0, 4.0, 6.0 and 8.0 cm as functions of time. The profiles are essentially the same up to 300 μs after the shock impact, with the magnitude in each plane increasing from the bottom wall to the top wall; this suggests that there are no significant three–dimensional effects through this time other than the diffusion of the SF_6 as it flows vertically. However, after 300 μs, differences between the profiles for each height appear, beginning with the profile near the top wall, and eventually spreading to lower heights.

We find that by the end of the simulation, the z-component of velocity has reached a maximum of 17 m/s, which is more than half of the maximum of the spanwise component. Positive z-velocity is maximum in the vortex cores, away from the upper and lower walls. Apparently, the stronger vortices near the upper wall have correspondingly lower core pressures compared to the weaker vortices near the lower wall; this pressure difference accelerates gas toward the upper wall through the vortex cores. The acceleration is compounded because the cores of the vortices are filled with air, and the heavier SF_6 is wrapped around the outside. The lighter air in the core of each vortex is inside a tube of SF_6, and is preferentially accelerated toward the upper wall. The different circulation profiles and large z-component of velocity suggest that three–dimensional effects are not negligible for the initial conditions we assumed. Only with experimental data can we test those assumptions.

5 Concluding Remarks

To date we have made a large number of two–dimensional simulations to validate the FLASH code for problems dominated by vortex dynamics. While this is work in progress, we can make the following remarks:

- The overall morphology of the flowfield is captured by the simulations, but differences exist in the location and extent of small–scale structure.
- Simulation velocity magnitudes lie within 10% of experimental values.
- For vortex–dominated subsonic flows, FLASH users should be cautious regarding the choice of CFL number, mesh refinement criteria, and if PPM is used, contact steepening.
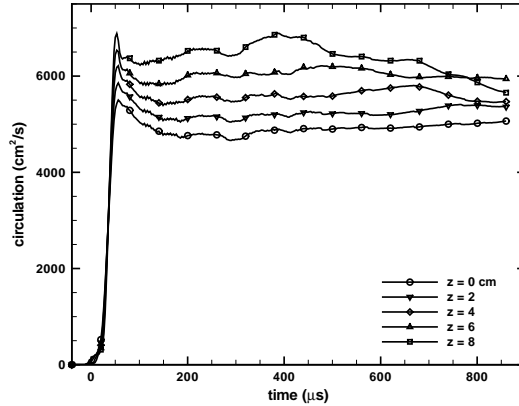
Fig. 9. Z–component of circulation in the lower-y half of the xy-plane at five vertical locations in the tunnel, as a function of time.

Our three–dimensional simulation, despite issues with the initial conditions, suggests that three–dimensional effects might be important for this experiment, and measurements should be made parallel to the cylinder axis to examine the issue.

References

1. J. W. Jacobs. The dynamics of shock accelerated light and heavy gas cylinders. *Physics of Fluids A*, 5(9):2239–2247, September 1993.
2. C. Tomkins et al. A quantitive study of the interaction of two Richtmyer-Meshkov-unstable gas cylinders. *Physics of Fluids*, 15(4):986–1004, April 2003.
3. C. A. Zoldi. *A Numerical and Experimental Study of a Shock-Accelerated Heavy Gas Cylinder*. PhD thesis, State University of New York at Stony Brook, 2002.
4. B. Fryxell et al. FLASH: An adaptive mesh hydrodynamics code for modeling astrophysical thermonuclear flashes. *ApJS*, 131:273–334, November 2000.
5. A. C. Calder et al. On validating an astrophysical simulation code. *ApJ Supplement Series*, 143:201–229, November 2002.
6. K. Prestridge et al. Validation of an instability growth model using particle image velocimetry measurements. *Phys. Rev. Lett.*, 84(19):4353–4356, May 2000.
7. K. T. Christensen et al. PIV sleuth: Integrated particle image velocimetry (PIV) interrogation/validation software. TAM report 943, UIUC, 2000.
8. T. Plewa. Parameter fitting problem for contact binaries. *Acta Astronomica*, 38:415–430, 1988.
9. J. J. Quirk and S. Karni. On the dynamics of a shock-bubble interaction. *Journal of Fluid Mechanics*, 318:129–163, 1996.
10. J. J. Quirk. *An Adaptive Mesh Refinement Algorithm for Computational Shock Hydrodynamics*. PhD thesis, Cranfield Institute of Technology, UK, 1991.
11. W. J. Rider et al. Statistical comparison between experiments and numerical simulations of shock-accelerated gas cylinders. In H. A. Mang et al., editor, *Proceedings of the Fifth World Congress on Computational Mechanics*, 2002.